Signal-to-noise ratio in dual-gated silicon nanoribbon field-effect sensors

A. Tarasov, W. Fu, O. Knopfmacher, J. Brunner, M. Calame, and C. Schönenberger[a)]
Department of Physics, University of Basel, Klingelbergstrasse 82, CH-4056 Basel, Switzerland

(Received 15 October 2010; accepted 13 December 2010; published online 7 January 2011)

Recent studies on nanoscale field-effect sensors reveal the crucial importance of the low-frequency noise for determining the ultimate detection limit. In this letter, the $1/f$-type noise of Si nanoribbon field-effect sensors is investigated. We demonstrate that the signal-to-noise ratio can be increased by almost two orders of magnitude if the nanoribbon is operated in an optimal gate voltage range. In this case, the additional noise contribution from the contact regions is minimized, and an accuracy of 0.5‰ of a pH shift in 1 Hz bandwidth can be reached. © *2011 American Institute of Physics*. [doi:10.1063/1.3536674]

During the past decade, there has been a growing interest in applying the concept of an ion-sensitive field-effect transistor[1,2] (FET) to nanoscale devices. It has been shown that carbon nanotube,[3–6] graphene,[7–9] nanowire,[10–12] and nanoribbon (NR)-FETs (Refs. 13 and 14) are especially promising for sensing applications. Compared to conventional FETs, nanoscaled devices provide a larger surface-to-volume ratio. This results in a high sensitivity of the overall FET channel conductance to changes in the surface potential caused by the adsorption of molecules.[15] In order to reach the detection limit, intense attempts have recently been made to understand the factors determining the signal-to-noise ratio (SNR).[9,16–18] Studies on carbon nanotube FETs (Ref. 17) and on nanowire FETs (Ref. 18) showed that the SNR increases in the subthreshold regime, which is therefore the preferred regime for high sensitivity. However, a more detailed understanding of the noise properties is needed to optimize the SNR across the full operating range of the FET.

In the present work, we measure the low-frequency $1/f$ noise of a dual-gated NR-FET (Refs. 17 and 19–21) in ambient and in a buffer solution and determine the resolution limit expressed in a noise equivalent threshold voltage shift δV_{th}, with the latter being the measurement quantity in these types of sensors. We identify two regimes which differ in the relative importance of the contact and intrinsic NR resistance. The lowest value in δV_{th} is found when the working point of the NR-FET is adjusted such that the intrinsic NR resistance dominates. In the other case when the contact resistance dominates the noise can be larger by almost two orders of magnitude for nominally the same overall resistance. This result shows the importance of being able to adjust the operating point properly. In the best possible case we determine a resolution limit of 0.5 ‰ of a pH change in 1 Hz bandwidth, which is comparable to a commercial pH meter [0.1 % (Ref. 22)], but for a much smaller active sensing area.

Silicon NR-FETs were produced by uv lithography[21] according to the top-down approach introduced by Nikolaides *et al.*[13] and further developed to nanowire FETs by Stern *et al.*[12] This high-yield process provides reproducible hysteresis-free FETs with the following dimensions: length $\times$ width $\times$ height $= 10\ \mu m \times 700\ nm \times 80\ nm$ [Fig. 1(a)]. A thin Al_2O_3 layer was deposited on the device to ensure leakage-free operation in an electrolyte solution. In addition, a liquid channel was formed in a photoresist layer, reducing the total area exposed to the electrolyte.

The measurement setup is schematically shown in Fig. 1(b). The NR-FETs were operated at low source-drain dc voltages $V_{sd}=10-100$ mV in the linear regime. The source-drain current I_{sd} through the NR was measured by a current-voltage converter with a variable gain $(10^5-10^9\ V/A)$. The conductance G of the NR-FET is then obtained as the ratio $G=I_{sd}/V_{sd}$ while varying both the backgate V_{bg} and liquid-gate voltage V_{lg}. This yields a two-dimensional conductance map, as shown in Fig. 1(c).[21] The vertical axis V_{ref} is the potential of the liquid, as measured by a calomel reference electrode. The equivalent voltage noise power spectral density S_V (see, e.g., Ref. 24) was determined along the solid

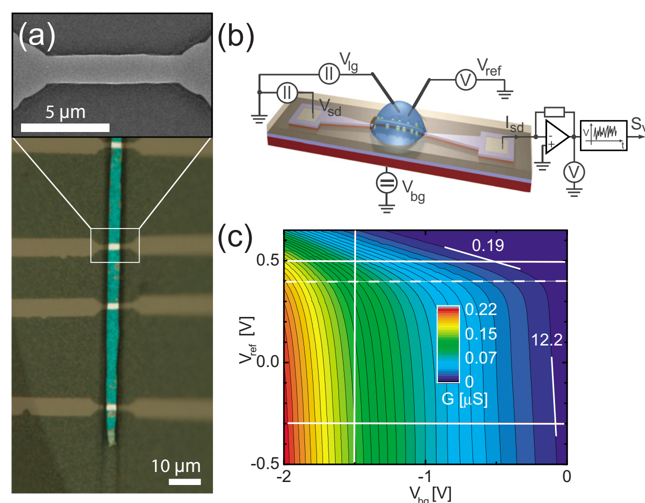

FIG. 1. (Color online) (a) Optical image of a sample with four NRs (horizontal) and an enlarged scanning electron microscope image of one of the NRs. The (vertical) liquid channel is the only part of the sample which is not covered with photoresist. (b) A schematic representation of the setup used for the measurements in liquid. There are two gates: a backgate and a liquid-gate with applied gate voltages V_{bg} and V_{lg}. The liquid potential is measured by a calomel reference electrode and denoted as V_{ref}. The NR-FETs are characterized by their small-signal conductance map $G(V_{bg},V_{ref})$, shown in (c), and by the noise obtained from the temporal dependence of the source-drain current I_{sd} using fast Fourier transform. In (c) the horizontal dashed line marks the border between two regimes: the NR- (upper) and contact- (lower) dominated regimes. Noise measurements were conducted along the three solid white lines. Short solid lines and numbers represent the slopes of the equiconductance lines.

[a)]Electronic mail: christian.schoenenberger@unibas.ch.

0003-6951/2011/98(1)/012114/3/$30.00 © 2011 American Institute of Physics

Downloaded 10 Jan 2011 to 131.152.227.74. Redistribution subject to AIP license or copyright; see http://apl.aip.org/about/rights_and_permissions

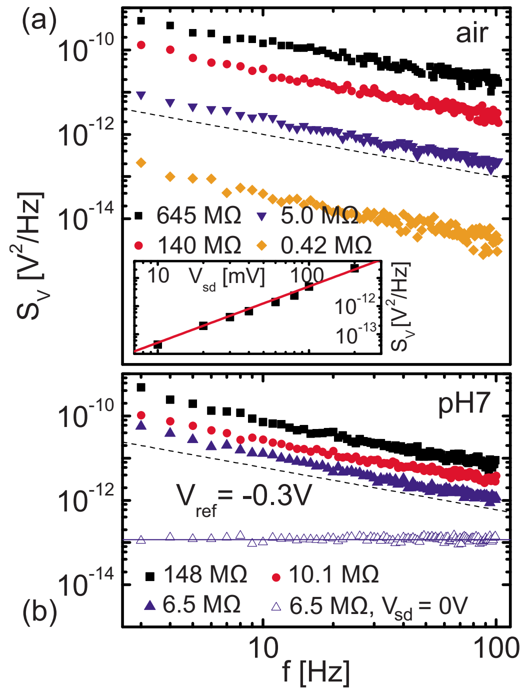

FIG. 2. (Color online) The noise power spectral density of the voltage fluctuations S_V obtained for a source-drain bias voltage of V_{sd}=90 mV for different resistances of a NR measured (a) in air and (b) in a buffer solution (Titrisol pH 7, Merck). The dashed lines indicate a $1/f$ slope. The open symbols in (b) represent the thermal noise of the NR at V_{sd}=0 V (△). The calculated thermal noise of a 6.5 MΩ resistor at 300 K is shown for comparison (horizontal line). Inset: S_V as a function of V_{sd} at 7 Hz, measured in air (logarithmic scale). The solid red line indicates a power law with exponent 2.

white lines through a fast Fourier transform of the time dependent fluctuations of I_{sd}.

The conductance map in Fig. 1(c) displays two different regimes, above and below the white dashed line at about V_{ref}=+0.4 V, which differ in their relative coupling to the two gates. This is visible in the slopes $s=\partial V_{ref}/\partial V_{bg}$ (short white lines and numbers), determined at constant G, which represent the ratio of the gate-coupling capacitances C_{bg}/C_{lg}, where C_{bg} denotes the backgate and C_{lg} denotes the liquid-gate capacitance.[21] To understand the origin of the two different regimes, one has to see that the NR-FET resistance $R=1/G$ is composed of two resistances in series: the intrinsic resistance R_{NR} and the contact resistance R_c. Due to the confinement of the liquid channel to the NR, R_c is only weakly affected by the liquid-gate (small C_{lg}). Hence, if R_c dominates R, C_{bg}/C_{lg} is large, which corresponds to the lower regime with $V_{ref}<0.4$ V. In contrast, if R_c can be neglected, R is determined by R_{NR}, which on its own is more strongly capacitively coupled to the liquid than to the backgate. We refer to the two regimes as contact- and NR-dominated.

Figure 2 shows the frequency dependence of the noise power $S_V(f)$ of the NR for different resistance values, measured in air [Fig. 2(a)] and in a buffer solution with pH 7 [Fig. 2(b)]. The corresponding thermal background noise, recorded at zero bias, has been subtracted from the data. An example is shown by △. $S_V(f)$ has a clear $1/f$ dependence (dashed lines), and its amplitude is proportional to V_{sd}^2 (inset), as expected for $1/f$ noise.[24] Such a behavior can phenomenologically be described by Hooge's law[23,24]

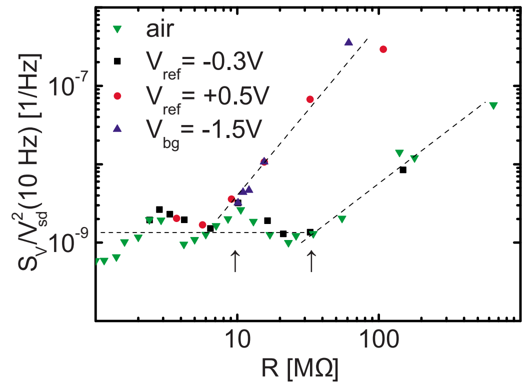

FIG. 3. (Color online) S_V divided by the squared source-drain voltage V_{sd}^2 as a function of R at 10 Hz, measured in air and in buffer solution (logarithmic scale). Dashed lines are guides to the eye. Arrows indicate the transition between different regimes.

$$S_V(f) = V_{sd}^2 \frac{\alpha}{Nf}. \quad (1)$$

The material dependent parameter α accounts for scattering effects and the constant N denotes the number of fluctuators in the system.

In Fig. 3, the normalized noise amplitude S_V/V_{sd}^2 at 10 Hz is depicted as a function of R. The noise in the system increases dramatically (indicated by dashed lines) above a certain threshold resistance value. The position of this threshold (arrows) and the steepness of the rise depend on whether the NR is gated by the liquid or the backgate. In air (▼), where V_{bg} is the only applied gate voltage, the noise starts to increase at roughly 30 MΩ. A similar behavior is observed in liquid in the contact-dominated regime, i.e., for V_{ref}=−0.3 V (■). In contrast, within the NR-dominated regime (●), the noise increases steeper, starting already at about 10 MΩ. For R smaller than the respective thresholds, the noise level is approximately constant. The apparent superimposed structure observed in this range is wire specific. Different NR-FETs, while confirming the general dependence, typically display a different fine structure. The thresholds of 10–30 MΩ correspond to the transition from the linear to the subthreshold regime of the FETs.

The physical signal in FET sensors is the shift ΔV_{th} of the threshold voltage V_{th} caused by a chemical change on the sensing surface. It is obtained from the measured conductance change ΔG and the transconductance $g=G'=dG(V_g)/dV_g$, characteristic for a given FET, as $\Delta V_{th}=\Delta G/g$. This equation can be used to determine the true figure of merit which is the equivalent noise power of the threshold voltage δV_{th} given by

$$\delta V_{th} = \frac{\sqrt{S_V/V_{sd}^2(f)}}{g/G} = \frac{\sqrt{S_V/V_{sd}^2(f)}}{(\ln G)'}. \quad (2)$$

Here, we have made use of the relation $\delta G/G=\sqrt{S_V}/V_{sd}$.

In Fig. 4(a) we show δV_{th} when the controlling gate is V_{bg} for data measured in air (▼) together with the data acquired in buffer solution at V_{ref}=−0.3 V (■). Both curves show a very similar behavior. Since we know that the liquid data obtained at V_{ref}=−0.3 V is contact-dominated, we conclude that the measurement in air is also contact-dominated.

In Fig. 4(b) we summarize δV_{th} for measurements done in an electrolyte. To obtain δV_{th}, we consistently use V_{lg} as

Downloaded 10 Jan 2011 to 131.152.227.74. Redistribution subject to AIP license or copyright; see http://apl.aip.org/about/rights_and_permissions

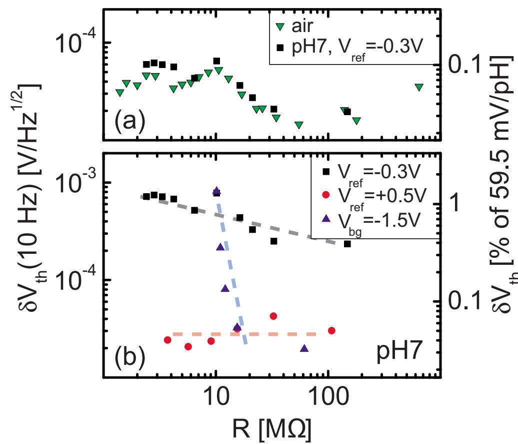

FIG. 4. (Color online) Threshold voltage fluctuations (a) $\delta V_{\mathrm{th}} = S_V/[\ln G(V_{\mathrm{bg}})]$ and (b) $S_V/[\ln G(V_{\mathrm{ref}})]$, calculated from the data in Fig. 3 as a function of R. Dashed lines are guides to the eye. The right axis shows δV_{th} relative to the Nernst limit of the pH sensitivity (59.5 mV/pH at 300 K).

the controlling gate for all three data sets in this figure. Interestingly, in the NR-dominated regime (●) δV_{th} is much smaller than in the contact-dominated regime (■). The difference can amount to almost two orders of magnitude. Although the voltage noise values S_V are not much different in the two regimes (Fig. 3), the sensitivities in the true measurement quantity greatly differ. This shows that the transconductance values, and therefore the gate-coupling to the liquid, are crucial factors determining the ultimate sensitivity. We also stress that δV_{th} can be low over an extended range of NR resistance values R, from ~ 1 to 100 MΩ. This range covers the transition from the linear to the subthreshold regime. The lowest value of $2\times 10^{-5}-3\times 10^{-5}$ V/$\sqrt{\mathrm{Hz}}$ corresponds to an accuracy of 0.5‰ of a typical Nernstian pH shift in 1 Hz bandwidth (right axis) throughout the full resistance range (●).

The data set obtained at a fixed V_{bg} and varying V_{ref} (▲) demonstrates the crossover between the two different regimes. In this case a very pronounced transition from a regime with low sensitivity (low R) to a regime with high sensitivity (larger R) is apparent. For this case, it has recently been pointed out[18] that the SNR (corresponding to $1/\delta V_{\mathrm{th}}$) increases with resistance R and is the highest in the subthreshold regime. We confirm this as well, but we emphasize that the dual-gate approach used here provides a more general and detailed insight. For $V_{\mathrm{ref}}=-0.3$ V, the contact leads also contribute to the total noise and strongly decrease the SNR. In contrast, for $V_{\mathrm{ref}}=+0.5$ V, the resistance of the NR-FET is not contact-dominated. In that case the SNR is constantly large over the whole resistance range.

As a last step, we estimate the charge noise of the NR, which corresponds to the minimum detectable number of charge carriers on the gate. To do so, we first define the gate-related power spectrum voltage noise $S_{\mathrm{Vg}}=S_I/g_m^2$. Here, $S_I=S_V/R^2$ is the current noise that can be easily determined from Fig. 3, and $g_m=\partial I/\partial V_g$ denotes the transconductance with respect to the controlling gate. For the measurement versus the liquid-gate ($V_{bg}=-1.5$ V), we obtain a charge noise at 10 Hz of $\sqrt{S_q}=C_{\mathrm{lg}}\sqrt{S_{\mathrm{Vg}}}/e\approx 5.8e/\sqrt{\mathrm{Hz}}$, where $C_{\mathrm{lg}} \approx 26$ fF is the estimated liquid-gate capacitance in our system and e is the elementary charge.

In conclusion, we have studied the low-frequency noise in dual-gated Si nanoribbon-FET sensors and determined the signal-to-noise ratio over a large resistance range. The deduced threshold voltage noise δV_{th} is an important quantity in a FET sensor and strongly depends on the working point. We stress that δV_{th} can be low over an extended range from the linear to the subthreshold regime, even though the voltage noise S_V grows nonlinearly with resistance and is the highest in the subthreshold range. We also confirmed recent studies that found the SNR increasing with resistance in a certain case.

The authors acknowledge the LMN at PSI Villigen for the oxidation of the SOI wafers. We are grateful for the support provided by the nano-tera.ch, Sensirion AG and the Swiss Nanoscience Institute (SNI). A.T. and W.F. contributed equally to this work.

[1] P. Bergveld, IEEE Trans. Biomed. Eng. **BME-17**, 70 (1970).
[2] P. Bergveld, Sens. Actuators B **88**, 1 (2003).
[3] S. Tans, A. Verschueren, and C. Dekker, Nature (London) **393**, 49 (1998).
[4] J. Kong, N. Franklin, C. Zhou, M. Chapline, S. Peng, K. Cho, and H. Dai, Science **287**, 622 (2000).
[5] P. Collins, K. Bradley, M. Ishigami, and A. Zettl, Science **287**, 1801 (2000).
[6] M. Krüger, M. R. Buitelaar, T. Nussbaumer, and C. Schönenberger, Appl. Phys. Lett. **78**, 1291 (2001).
[7] P. Ang, W. Chen, A. Wee, and K. Ping, J. Am. Chem. Soc. **130**, 14392 (2008).
[8] Y. Ohno, K. Maehashi, Y. Yamashiro, and K. Matsumoto, Nano Lett. **9**, 3318 (2009).
[9] Z. Cheng, Q. Li, Z. Li, Q. Zhou, and Y. Fang, Nano Lett. **10**, 1864 (2010).
[10] X. Duan, Y. Huang, Y. Cui, J. Wang, and C. Lieber, Nature (London) **409**, 66 (2001).
[11] Y. Cui and C. Lieber, Science **291**, 851 (2001).
[12] E. Stern, J. F. Klemic, D. A. Routenberg, P. N. Wyrembak, D. B. Turner-Evans, A. D. Hamilton, D. A. LaVan, T. M. Fahmy, and M. A. Reed, Nature (London) **445**, 519 (2007).
[13] M. G. Nikolaides, S. Rauschenbach, and A. R. Bausch, J. Appl. Phys. **95**, 3811 (2004).
[14] N. Elfström, A. E. Karlström, and J. Linnros, Nano Lett. **8**, 945 (2008).
[15] N. Elfström, R. Juhasz, I. Sychugov, T. Engveldt, A. Eriksson, and J. Linnros, Nano Lett. **7**, 2608 (2007).
[16] N. K. Rajan, D. A. Routenberg, J. Chen, and M. Reed, IEEE Electron Device Lett. **31**, 615 (2010).
[17] I. Heller, J. Männik, S. G. Lemay, and C. Dekker, Nano Lett. **9**, 377 (2009).
[18] X. A. Gao, G. Zheng, and C. Lieber, Nano Lett. **10**, 547 (2010).
[19] O. Elibol, B. Reddy, Jr., and R. Bashir, Appl. Phys. Lett. **92**, 193904 (2008).
[20] O. Knopfmacher, D. Keller, M. Calame, and C. Schönenberger, Procedia Chem. **1**, 678 (2009).
[21] O. Knopfmacher, A. Tarasov, W. Fu, M. Wipf, B. Niesen, M. Calame, and C. Schönenberger, Nano Lett. **10**, 2268 (2010).
[22] Microsens SA, http://www.microsens.ch/products/pdf/MSFET_datasheet%20.pdf (retrieved 17 September 2010).
[23] F. N. Hooge, Phys. Lett. **29A**, 139 (1969).
[24] F. N. Hooge, T. G. M. Kleinpenning, and L. K. J. Vandamme, Rep. Prog. Phys. **44**, 479 (1981).

Downloaded 10 Jan 2011 to 131.152.227.74. Redistribution subject to AIP license or copyright; see http://apl.aip.org/about/rights_and_permissions